

# Simple o3: Towards Interleaved Vision-Language Reasoning

Ye Wang<sup>1</sup>, Qianglong Chen<sup>\*</sup>, Zejun Li<sup>1</sup>, Siyuan Wang<sup>2</sup>,  
 Shijie Guo<sup>1</sup>, Zhirui Zhang<sup>\*</sup>, Zhongyu Wei<sup>1</sup>

<sup>1</sup>Fudan University

<sup>2</sup>University of Southern California

yewang22@m.fudan.edu.cn,

{chenqianglong.ai, zrustc11}@gmail.com,

{zejunli20, guoshijie, zywei}@fudan.edu.cn,

sw\_641@usc.edu

## Abstract

Multimodal Large Language Models (MLLMs) have shown impressive performance on vision-language tasks, but their long Chain-of-Thought (CoT) capabilities in multimodal scenarios remain underexplored. Inspired by OpenAI’s o3 model, which emulates human-like “thinking with image” through iterative visual transformations and linguistic reasoning, we propose Simple o3, an end-to-end framework that integrates dynamic tool interactions (e.g., cropping, zooming, and reusing) into interleaved vision-language reasoning via supervised fine-tuning (SFT). Our approach features a scalable data synthesis pipeline that generates high-quality interleaved vision-language reasoning chains via an “observe-reason-act” cycle, complete with executable visual operations and rigorous verification, yielding the open-source TWI-Tools-146K dataset. Experimental results demonstrate Simple o3’s superior performance on diverse benchmarks, outperforming existing approaches. By combining enhanced reasoning capabilities, Simple o3 establishes a powerful yet computationally affordable paradigm for advancing multimodal reasoning. Remarkably, we provide the first in-depth analysis of different interleaved reasoning strategies, offering insights into their impact on model performance. We found that by introducing additional visual tokens for interleaved vision-language reasoning, reusing and magnifying the original image significantly improves the model’s visual reasoning and fine-grained perception, while image cropping based on precise visual grounding allows the model to effectively focus on key entities or regions, further enhancing its capabilities.

## Introduction

Recent advancements in Multimodal Large Language Models (MLLMs) have demonstrated remarkable proficiency across a wide range of vision-language tasks (Bai et al. 2025a; Chen et al. 2024b; Liu et al. 2024a; Li et al. 2024a; Team et al. 2025), from image captioning to visual question answering (VQA). Concurrently, the exploration into “slow-thinking” capabilities in large language models (LLMs), inspired by human deliberative reasoning processes, has gained traction. (Wei et al. 2022; Kojima et al. 2022; Guo et al. 2025; Yu et al. 2025).

However, research on extended Chain-of-Thought (CoT) in multimodal scenarios—particularly those involving in-

terleaved visual-language reasoning pathways—remains largely underexplored. A seminal advance in this direction is OpenAI’s newly proposed O3 model, which emulates human-like reasoning by “thinking with images”—an iterative paradigm where visual perception and cognitive processing co-evolve. At each reasoning step, the model transforms images (e.g., by cropping, zooming, or rotating), concurrently performing linguistic reasoning to plan subsequent visual operations. This forms a groundbreaking framework for multimodal agentic reasoning, bridging continuous visual and discrete linguistic reasoning. While tool-augmented reasoning has demonstrated promise in language-only domains (Li, Zou, and Liu 2025; Jin et al. 2025), there lacks a systematic methodology to activate such capabilities in multimodal scenarios that could enable hierarchical task decomposition, akin to how humans revisit and manipulate visual stimuli during complex problem-solving. Second, current approaches for eliciting tool-use behaviors in MLLMs rely heavily on resource-intensive Reinforcement Learning (RL) or human annotation, lacking scalable pipelines for synthesizing high-quality interleaved vision-language reasoning data (Liu et al. 2025b; Fan et al. 2025; Liu et al. 2025a). Moreover, which tools can effectively enhance multimodal reasoning capabilities and how input resolution affects interleaved vision-language reasoning remain underexplored. Addressing this gap is key to optimizing visual information usage and advancing model reasoning capabilities.

In this paper, we introduce Simple o3, a simple yet powerful open-source framework for end-to-end learning of tool-augmented reasoning with interleaved image-text inputs. The framework combines a scalable data generation pipeline, a training method that incorporates image masking, and a multi-step reasoning enabling seamless tool interaction, offering an integrated solution for complex multimodal tasks. Specifically, we propose a scalable, high-quality data synthesis pipeline that automatically generates interleaved vision-language reasoning chains through an iterative “observe-reason-act” cycle. Given a question-image pair, the pipeline first produces atomic reasoning steps alongside corresponding visual operation plannings, then converts these plannings into executable parameters for precise image transformations (e.g., *focus\_area*, *zoom\_in*, or *reuse*). Using designated visual tools, the system applies

<sup>\*</sup>Independent Researcher

these parameters to update the visual state, iteratively repeating the cycle until the accumulated reasoning steps provide sufficient evidence to trigger the answer. Meanwhile, the two-step verification module ensures semantic consistency between visual operation planning and output parameters while filtering out answers inconsistent with the ground truth, thereby maximizing the retention of high-quality data. During training, we reformat the multi-turn dialogue data into a single-turn user-assistant structure, unify coordinate systems, and apply image masking for loss computation. During inference, the model detects parameters within function tags at each step, executes the corresponding image operations, and iterates until the answer is derived. This tool-interactive approach to interleaved image-text reasoning substantially enhances the model’s logical capabilities, as demonstrated in Figure 1.

Our main contributions are fourfold: (1) We propose Simple o3, which reproduces and extends the o3 model’s tool-interactive “thinking with images” paradigm, advancing the development of multimodal CoT reasoning. (2) We introduce an iterative, high-quality data synthesis pipeline, providing detailed methodology for generating image-text interleaved reasoning data with executable function calls, accompanied by the release of our open-source TWI-Tools-146K dataset. (3) Experimental results demonstrate that Simple o3 achieves significant improvements on multimodal reasoning and perception benchmarks, validating the effectiveness of our approach. (4) We present the first in-depth analysis of the impact of tool selection and input resolution on interleaved vision-language reasoning performance, providing key insights for future “thinking with images” research.

## Related Work

### Multi Large Language Models

By integrating visual encoders with powerful LLMs, MLLMs gain visual perception capabilities (Alayrac et al. 2022; Awadalla et al. 2023). Early MLLMs primarily followed architectures like LLaVA (Liu et al. 2024b) and BLIP-2 (Li et al. 2023a), employing either MLP-based or attention-based connector modules to bridge the visual and language modalities (Zhu et al. 2023; Bai et al. 2023; Chen et al. 2023). In these frameworks, the visual encoder processes an input image, after which the connector module projects the visual features to align dimensionally with text embeddings, forming a unified multimodal sequence representation. Since most visual encoders are constrained by fixed input resolutions and capturing only partial visual features, subsequent research has prioritized enhancing visual representations. Two predominant approaches have emerged: some directly extend the visual encoders’ capabilities (Yuan et al. 2024; Ge et al. 2024; Fan et al. 2024), and others adopt dynamic resolution strategies that process high-resolution images by decomposing them into multiple sub-images while simultaneously analyzing downsampled global views through low-resolution encoders (Ye et al. 2023a; Li et al. 2024c,a; Chen et al. 2024b). While these innovations have substantially improved visual perception, the persistent limitations in reasoning capacity continue to

constrain overall model performance.

### Long CoT in MLLMs

Early MLLMs predominantly adopted a two-stage training paradigm consisting of vision-language pretraining followed by instruction fine-tuning (Dai et al. 2023; Liu et al. 2023; Ye et al. 2023b; Zeng et al. 2024). While this approach improved instruction-following capabilities, it inherently separates perception from reasoning. Subsequent research has sought to address this limitation by integrating various forms of textual auxiliary inputs, including detailed reasoning traces, spatial coordinates, attribute relations, and comprehensive image descriptions, to provide evidential grounding for model outputs (Shao et al. 2024; Xu et al. 2024). The emergence of DeepSeek-R1 marked a turning point where RL became a key enabler for reasoning enhancement, spawning diverse training paradigms. Similar advancements soon appeared in multimodal domains. While recent research has increasingly focused on reward signal design (Huang et al. 2025; Liu et al. 2025c; Zhang et al. 2025b; Zhou et al. 2025), OpenAI’s o3 model pioneered the ‘thinking with images’ paradigm and has gradually become pivotal for enhancing multimodal reasoning capabilities (Zhang et al. 2025a; Wang et al. 2025a; Bai et al. 2025b; Ni et al. 2025; Chung et al. 2025). Approaches like Deep-Eyes (Zheng et al. 2025) and Chain-of-Focus (Zhang et al. 2025c) dynamically leverage image cropping tools to facilitate adaptive visual reasoning (Zhu et al. 2025; Su et al. 2025). However, these works constrain the reasoning process to basic image cropping operations. This limited toolset results in rigid inference pipelines that lack adaptability to diverse scenarios, where different tasks may require distinct visual processing strategies. More critically, existing work fails to systematically examine how tool selection and input resolution influences fundamental model capabilities, particularly in perceptual understanding and reasoning.

## Simple o3

In this section, we introduce Simple o3 through three key components: (1) the scalable data generation pipeline that automates high-quality reasoning chain creation, (2) the novel training methodology incorporating image masking, and (3) the multi-step inference enabling dynamic tool interaction. These components collectively form an end-to-end system for interleaved image-text reasoning, achieving robust performance through adaptive multi-tool collaboration.

### Scalable Data Generation Pipeline

We propose a data generation pipeline consisting of a reasoning path generator and a two-step verification module, as shown in Figure 4. In the generation phase, the MLLM serves as an orchestrator that dynamically analyzes task requirements and coordinates predefined visual tools: *focus\_area* returns the image with a drawn bounding box (bbox) of a focused region, *zoom\_in* magnifies the whole image area via interpolation, and *reuse* directly outputs the original image. Each tool encapsulates a dedicated image

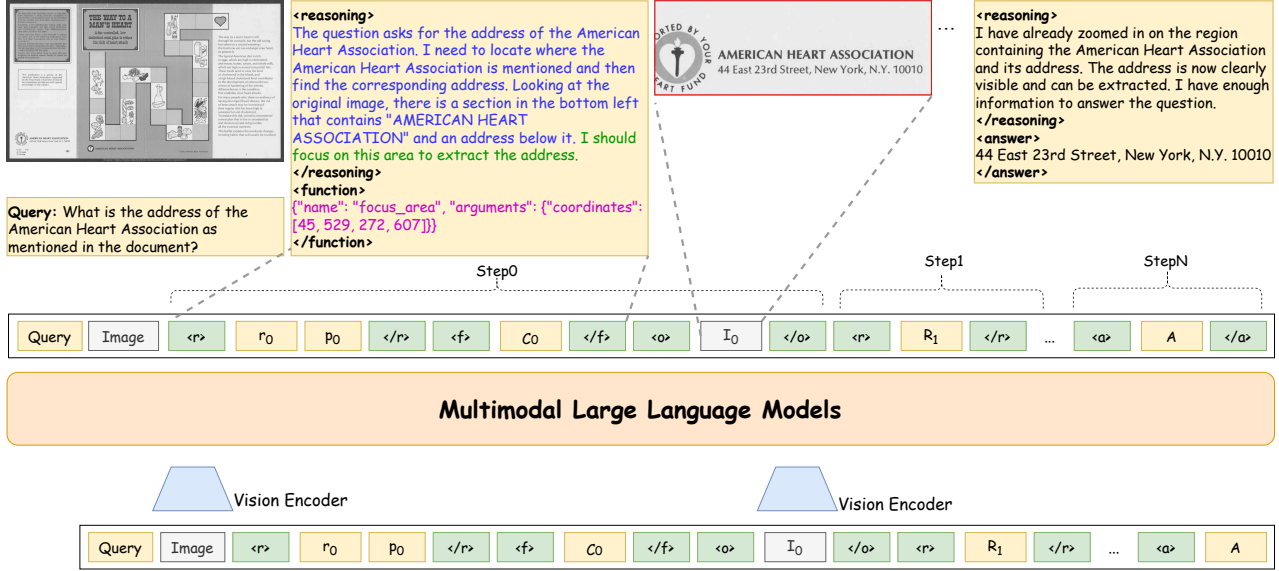


Figure 1: Overview of Simple o3. At Step 0, the blue text represents the atomic reasoning step  $r_0$ , while the green text represents the visual operation plan  $p_0$ . These two components constitute the reasoning content  $R_0$ . The pink text represents the tool instruction  $C_0$ , which is returned as JSON object. During training, *focus\_area* operation is followed by an image with the bbox to obtain the complete visual information of the image. During inference, the image is cropped according to the coordinates returned by *focus\_area* to inject visual tokens of target entities or regions.

processing function, which can perform the atomic manipulation on the input image. We employ *gemini-2.5-Flash-Preview-05-20* in its non-thinking mode to optimize the trade-off between generation efficiency and computational overhead. The reasoning path generation follows an iterative cycle:

$$S = \{s_0, s_1, \dots, s_t, A\} \quad (1)$$

$$s_t = (R_t, C_t, I_t) \sim P(\cdot \mid Q, I, H_{t-1}; \theta_{MLLM}) \quad (t \geq 0) \quad (2)$$

$$H_{t-1} = \begin{cases} \emptyset & \text{if } t = 0, \\ \{(R_i, C_i, I_i)\}_{i=0}^{t-1} & \text{if } t \geq 1. \end{cases} \quad (3)$$

Here,  $S$  represents the iterative reasoning chain comprising the serialized atomic reasoning step  $s$ , and final answer  $A$ .  $s_t$  denotes the output at reasoning step  $t$ , including the reasoning content  $R_t$ , the tool command  $C_t$ , and the returned image  $I_t$ , formed as the triple, by sampling from the MLLM while considering the historical reasoning path  $H_{t-1}$  that aggregates all previous steps' information as the reasoning process unfolds.

Our pipeline utilizes structured tags as special tokens to delineate distinct reasoning components. The reasoning content  $R_t = (r_t, p_t)$ , comprising atomic reasoning steps  $r_t$  and visual planning  $p_t$ , is encapsulated within  $\langle reasoning \rangle$  and  $\langle /reasoning \rangle$  tags. Tool invocations  $C_t = (T_n, Param)$ , specifying both operation names and input parameters, are marked by  $\langle function \rangle$  and  $\langle /function \rangle$  tags. The system dynamically generates new visual states through image manipulations, with the resulting transformed images

being encoded and embedded between  $\langle observation \rangle$  and  $\langle /observation \rangle$  delimiters. This structured tagging scheme preserves a complete and parseable record of multimodal reasoning chain progression.

The verification process begins by assessing the geometric validity of tool interactions using *gemini-2.5-flash-lite-preview-06-17*. For *focus\_area*, we retain samples where the bbox either precisely matches or fully contains the target entity. *zoom\_in* and *reuse* operations are validated based on semantic consistency between the tool command  $C_t$  and the visual planning description  $p_t$ . Finally, the answer is verified by comparing system outputs against ground truth using *Qwen3-turbo*. For each question-image-answer triplet, the MLLM constructs a multi-step reasoning chain, potentially invoking visual tools. The system performs a maximum of two generation attempts per sample to enhance validity.

## TWI-Tools-146K Data Curation

We carefully curate the dataset from diverse tasks to maximize the data distribution, thereby enhancing Simple o3's generalization capability. Our TWI-Tools-146K training dataset is sourced from following datasets: MATHV360K (Shi et al. 2024), LLaVA-CoT-100K (Xu et al. 2024), and ArxivQA (Li et al. 2024b). We exclude sub-tasks including math problems from MATHV360K, as geometry typically focuses more on the extension of textual tokens. Through proportional sampling across remaining sub-datasets, we initially generate 150K candidate entries. After rigorous verification, we retain approximately 100K high-quality samples, covering perceptual VQA, knowledge-based reasoning, chart analysis, and logical reasoning, rep-

resenting a comprehensive collection of challenging real-world tasks. To establish robust visual understanding capabilities, we primarily select COCO QA pairs from LLaVA-CoT-100K, generating 27K samples featuring diverse real-world imagery. To further enhance abstract figure interpretation and reasoning, we extract 19K proportionally balanced samples from ArxivQA, covering all subcategories.

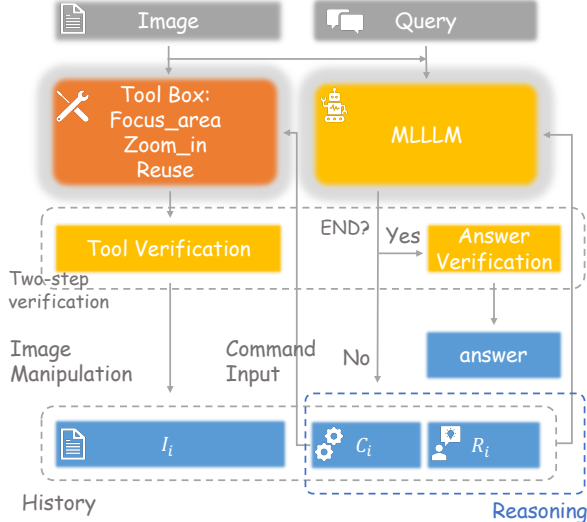


Figure 2: Overview of scalable data generation pipeline. MLLM generates current reasoning content and tool commands at each step. The toolbox processes input images based on these commands, returning manipulated visuals, followed by tool verification to ensure semantic alignment between commands and visual operations. Upon successful verification, the system combines the current step’s generation into the history, for the next generation step. This cycle repeats until the answer is generated, concluding with answer verification to produce a complete data sample.

## Training Incorporating Image Masking

Our data generation pipeline produces interleaved vision-language sequences  $Z = (Q, I, S)$ , where the iterative reasoning chain  $S$  can be further decomposed into individual elements  $z_t$  from different modalities, originating from the text space  $\mathcal{T}$  or the visual space  $\mathcal{V}$ . To adapt the multi-turn “user-assistant-tool” dialogues obtained during data generation into a suitable training format, we consolidate their reasoning paths into single-turn “user-assistant” sequences. Prior to training, we also resolve potential coordinate system discrepancies by converting all spatial coordinates to the native representation format of the target model. For effective learning from multimodal reasoning sequences  $S = (z_0, \dots, z_t)$ , we employ a selective loss computation mechanism governed by modality-aware masking  $M_t$ , which ensures proper gradient flow while maintaining cross-modal interactions.

$$M_t = \begin{cases} 1 & \text{if } z_t \in \mathcal{T} \text{ (compute loss)} \\ 0 & \text{if } z_t \in \mathcal{V} \text{ (ignore loss)} \end{cases} \quad (t \geq 0) \quad (4)$$

The training objective employs a masked cross-entropy loss that optimizes textual generation, zeroing out gradients for visual tokens:

$$\mathcal{L}_{SFT} = - \sum_{t=0}^T M_t \cdot \log P(z_t | Q, I, H_{t-1}; \theta_{MLLM}), \quad (5)$$

where the history  $H_{t-1}$  is defined as:

$$H_{t-1} = \begin{cases} \emptyset & \text{if } t = 0, \\ \{z_i\}_{i=0}^{t-1} & \text{if } t \geq 1. \end{cases} \quad (6)$$

In our implementation, visual tokens are demarcated by special tokens like  $<|image\_pad|>$  and serve only as contextual inputs. The binary mask ensures the model attends to visual data for understanding while restricting gradient updates to textual outputs.

## Multi-step Inference with Tool Interaction

After supervised fine-tuning, the model demonstrates proficiency in processing structured formats, enabling tool usage and multi-step interleaved vision-language reasoning. This capability facilitates dynamic alternation between text and image token generation until reaching an answer or hitting the round limit. The workflow is depicted in Algorithm 1: At each reasoning step  $t$ , the model outputs the reasoning content between  $<reasoning>$  and  $</reasoning>$  tags. Upon detecting the  $</function>$  token, the system automatically pairs it with the preceding  $<function>$  tag and extracts the JSON-formatted tool command  $C_t$ . Note that during inference, *focus\_area* crops the image based on the returned coordinates instead of outputting the full image with a drawn bbox. This command is then passed to a predefined function for visual processing, and the resulting image  $I_t$  is embedded as visual tokens between  $<observation>$  and  $</observation>$  tags before being appended to the model’s history. Finally, the model performs summary reasoning and outputs the answer between  $<answer>$  and  $</answer>$  tags, completing the inference cycle.

## Experiments

### Experimental Setup

**Implementation Details** We perform full parameter fine-tuning on Qwen2.5-VL-7B (Bai et al. 2025a) using TWI-Tools-146K data, with a mixture of partial general reasoning data. The maximum sequence length is set to 8,192 tokens. Input images are resized to a resolution range between a minimum of  $4 \times 28 \times 28$  pixels and a maximum of  $1024 \times 28 \times 28$  pixels. We employ a cosine learning rate scheduler with an initial rate of  $1.0e-5$  and 10% warmup ratio, training for 1 epoch with the batch size of 8. The vision encoder and multi-modal projector remain frozen during training.

---

**Algorithm 1: MLLM Response with Multi-Turn Inference**

**Require:** Input query  $Q$ , Input image  $I$ , MLLM  $\pi_\theta$ , tool box  $\mathcal{T}$ , maximum rounds  $M$ .

**Ensure:** Final response  $S$ .

```

1: Initialize multimodal reasoning sequence  $S \leftarrow \emptyset$ 
2: Initialize round count  $r \leftarrow 0$ 
3: while  $r < M$  do
4:   Generate response token  $y_t \sim \pi_\theta(\cdot | Q, I, S)$   $\triangleright$ 
   Append  $y_t$  to multimodal sequence  $S$ 
5:    $S \leftarrow S + y_t$ 
6:   if  $\langle \text{function} \rangle \langle / \text{function} \rangle$  detected in  $y_t$  then  $\triangleright$ 
   Extract tool command  $C_t$ 
7:      $C_t \leftarrow \text{Parse}(\langle \text{function} \rangle, y_t, \langle / \text{function} \rangle)$   $\triangleright$ 
   Retrieve tool instruction
8:      $I_t = \mathcal{T}(I, C_t)$   $\triangleright$  Image operation using the tool
   box
9:      $S \leftarrow S + \langle \text{observation} \rangle I_t \langle / \text{observation} \rangle$ 
10:    Increment round  $r \leftarrow r + 1$ 
11:   end if
12:   if  $\langle \text{answer} \rangle \langle / \text{answer} \rangle$  detected in  $S$  then  $\triangleright$ 
   Terminate generation
13:     return final generated response  $S$ 
14:   end if
15: end while
16: return final generated response  $S$ 

```

---

**Baselines and Benchmarks** We compare Simple o3 with proprietary models like GPT-4o (Hurst et al. 2024) and 4o-mini, as well as competitive open-source models, LLaVA-OneVision-7B (Li et al. 2024a) and Ovis1.6-Gemma2-9B (Lu et al. 2024). We additionally evaluate it against other models adopting the “thinking with images” paradigm, including DeepEyes (Zheng et al. 2025) and Chain-of-Focus (Zhang et al. 2025c). To validate the effectiveness of Simple o3, we evaluate it on multimodal reasoning benchmarks, including the reasoning subtasks in MME (Fu et al. 2024) and reasoning questions in CharXiv (Wang et al. 2024), VisuLogic (Xu et al. 2025), as well as fine-grained perception benchmarks such as HR-Bench 4K (Wang et al. 2025b), VStarBench (Wu and Xie 2024), and COCO Caption (Chen et al. 2015). Additionally, we assess its performance on general VQA tasks like ScienceQA (Saikh et al. 2022), MMStar (Chen et al. 2024a), and MMVet (Yu et al. 2024). Beyond these comprehensive evaluations, we also test the model on hallucination benchmarks, including POPE (Li et al. 2023b) and HallusionBench (Guan et al. 2024), and chart comprehension tasks such as DocVQA (Mathew, Karatzas, and Jawahar 2021) and InfoVQA (Mathew et al. 2022).

## Main Experiments

By delving into the performances in Table 1, we conclude that Simple o3 achieves significant improvements on multimodal reasoning benchmarks. Notably, on the MME reasoning subset, Simple o3 outperforms the base model by nearly 50 points—a margin that even surpasses GPT-4o by 27 points. This strongly demonstrates the effectiveness of

“thinking with images” where increasing the number of attended visual tokens enhances the model’s reasoning capability. Additionally, our method achieves improvements of 4.2% and 3.3% on CharXiv and VisuLogic respectively. For cases involving multiple abstract entities in images, the model leverages its robust grounding capability to locate relevant sub-regions, and through multi-step atomic reasoning, it gradually approaches the correct answer.

For multimodal perception, COCO Caption focuses on coarse-grained perception, evaluating a model’s holistic understanding of images. Compared to the base model, Simple o3 improves performance by 3.1 points by leveraging increased reuse of the original image to enhance detailed comprehension during inference. Meanwhile, HR-Bench 4K and VStarBench involve high-resolution images where target objects may occupy only a small fraction of pixels, emphasizing fine-grained perception. Our method achieves superior performance, approximately 7.4% and 12.9%, on these fine-grained benchmarks, outperforming existing approaches. Beyond the significant improvements in fine-grained perception, as shown in Table 3, we also observe that the model exhibits strong advantages in handling spatial reasoning tasks, particularly on subtasks of MMVet and LogicVista, achieving improvements of 16.6% and 10.3%. This suggests that our vision-language interleaved reasoning approach enhances the model’s understanding of relationships between different entities or areas. By accurately predicting the positional information of target objects and extracting visual features from relevant regions, the model achieves a unified comprehension of object locations across both language and visual modalities.

We also compare Simple o3 with two RL-based approaches, DeepEyes and Chain-of-Focus, which both employ the ‘Crop-then-Resize’ strategy in Table 4. Our method demonstrates superior performance on both HR-Bench 4K and VStarBench, further validating the effectiveness of the “thinking with images” in visual reasoning. Although Simple o3 does not achieve the best performance compared to other methods in POPE, it still improves on two hallucination benchmarks, especially by 2.3% in HallusionBench.

In general VQA benchmarks, as shown in Table 2, Simple o3 demonstrates consistent superiority over Qwen2.5-VL-7B. In ScienceQA, Simple o3 achieves 90.0%, outperforming by 1.3%, which reflects its stronger capability in integrating multidisciplinary knowledge for multimodal QA. The model further exhibits enhanced real-world applicability with a 1.1% improvement on RealWorldQA, showcasing superior generalization in practical scenarios. Notably, Simple o3 advances multimodal integration with significant gains of 2.6 and 1.5 points on MMStar and MMVet respectively, proving its exceptional effectiveness in fusing visual-language data and handling complex multimodal tasks through refined multidimensional capability alignment. Although the performance of foundation models on the DocVQA benchmark has nearly reached saturation at 94.7%, Simple o3 still maintains its performance lead through fine-tuning. Meanwhile, its improvement on the InfoVQA benchmark demonstrates significantly enhanced capabilities in parsing key information from charts.

Model	Reasoning			Perception			Hallucination	
	MME(R)	CharXiv	VisLog	HR-4K	V*	COCOC	POPE	HalB
GPT-4o*	674.6	29.9	25.1	46.8	45.0	23.1	84.6	44.2
GPT4o-mini*	564.3	32.7	25.8	48.0	50.8	17.4	83.3	39.3
Ovis1.6-7B*	547.5	36.5	-	64.1	71.2	14.4	87.8	44.1
LLaVA-OV-9B*	415.4	22.4	22.5	64.7	72.8	9.9	88.3	30.3
Qwen2.5-VL-7B*	652.5	37.6	26.0	68.8	77.5	15.0	86.0	42.1
Simple o3*	702.1	41.8	29.3	76.2	90.4	18.1	87.6	44.4
$\Delta$ (vs Base)	+49.6	+4.2	+3.3	+7.4	+12.9	+3.1	+1.6	+2.3

Table 1: Comparison results on multimodal reasoning benchmarks: reasoning tasks in MME, CharXiv(val), and VisuLogic, perception benchmarks: HR-Bench 4K, VStarBench, and COCO Caption(val), and hallucination benchmarks: POPE and HallusionBench. We use Rouge-L scores for COCO Caption. For HallusionBench, we report the mean accuracy of unique questions and all figures. \* denotes the result is reproduced by ourselves. For HR-Bench 4K, VStarBench, and POPE, the highest input resolution is set to  $16384 \times 28 \times 28$ , and for other benchmarks, it is set to  $2048 \times 28 \times 28$ .

Model	General VQA				Chart	
	Sci-QA	RW-QA	MM*	MMVet	DocVQA	InfoVQA
GPT-4o*	88.4	67.2	61.5	68.6	55.5	38.9
GPT4o-mini*	85.6	66.7	54.5	69.8	78.0	57.9
Ovis1.6-9B*	93.3	71.0	62.6	61.9	88.9	73.4
LLaVA-OV-7B*	95.3	69.7	61.9	52.7	87.0	66.4
Qwen2.5-VL-7B*	88.7	68.4	63.9	68.2	94.7	80.0
Simple o3*	90.0	69.5	66.5	69.7	94.8	82.0
$\Delta$ (vs Base)	+1.3	+1.1	+2.6	+1.5	+0.1	+2.0

Table 2: Comparison results on general VQA benchmarks: ScienceQA, RealWorldQA, MMStar, and MMVet, and chart comprehension benchmarks: DocVQA(val) and InfoVQA(val). The highest input resolution is set to  $2048 \times 28 \times 28$ .

Model	VisuLogic Spatial	MMVet rec_spat	LogicVista spatial
Qwen2.5-VL-7B*	22.9	66.7	20.5
Simple o3*	26.4	83.3	30.8
$\Delta$ (vs Base)	+3.5	+16.6	+10.3

Table 3: The performance of Simple o3 on spatially relevant benchmarks.

Model	HR-Bench 4K	POPE	V*Bench
Qwen2.5-VL-7B*	68.8	86.0	77.5
DeepEyes	75.1	87.7	90.1
Chain-of-Focus	-	88.4	88.0
Simple o3*	76.2	87.6	90.4
$\Delta$ (vs Best)	+1.1	-0.8	+0.3

Table 4: Comparative performance of Simple o3 with other interleaved vision-language reasoning methods: DeepEyes and Chain-of-Focus.

## Ablation Study

For the ablation study, we select representative benchmarks from key categories including multimodal reasoning, perception, hallucination, and chart understanding. We analyze the impact of visual manipulation tools in Table 5, by incrementally incorporating components, beginning with *reuse*, to quantify their cumulative contributions. Experiments demonstrate that the *reuse* operation delivers significant performance improvements, achieving gains of 31.2 points on MME and 4.8% on VStarBench, with at least 1-point improvements on other benchmarks. This indicates that *reuse* enhances the model’s perception and reasoning capabilities through the introduction of additional visual tokens. While all operations contribute positively to performance, the *zoom\_in* operation yields marginal benefits (mostly below 1%) except on VStarBench. *focus\_area* emerges as another critical tool, particularly excelling in fine-grained perception tasks like HR-Bench 4K and VStarBench with improvements of 4.9% and 6.9% respectively. Its advantage lies in precise visual localization that eliminates redundant visual information while focusing on key entities or regions, thereby delivering consistent performance gains. These findings suggest that the synergistic combination of these three tools elevates the model’s reasoning upper bound.

Further, our analysis extends to the role of heterogeneous training data in shaping model capabilities, as summarized in Table 6. First, general reasoning data results in a slight overall boost in model performance. MATHV360K broadens the data distribution by introducing complex visual QA, charts, logical reasoning problems. This leads to a performance leap of nearly 27 points on the MME reasoning task, alongside gains of 1.3% on CharXiv and 0.9% on InfoVQA. We attribute this to the large scale of complex VQA and chart data, which strengthen the model’s representation of logical inter-object relations, thereby refining its strategic planning for visual tool operations. Concurrently, the logic-centric tasks directly bolster its atomic reasoning capabilities. However, a relative dearth of perceptual samples in the initial training mix results in modest gains on fine-grained perception benchmarks, including HR-Bench 4K, VStarBench, and HallusionBench. To remediate this deficit,

Model	MME(R)	CharXiv	HR-4K	V*	HalB	InfoVQA
Qwen2.5-VL-7B	652.5	37.6	68.8	77.5	42.1	80.0
+ w/ <i>reuse</i>	683.7	39.0	70.5	82.3	43.3	81.6
++ w/ <i>zoom_in</i>	689.6	39.6	71.3	83.5	43.7	81.8
+++ w/ <i>focus_area</i>	<b>702.1</b>	<b>41.8</b>	<b>76.2</b>	<b>90.4</b>	<b>44.4</b>	<b>82.0</b>

Table 5: Performance comparison of tool implementations variants: Only *reuse*, plus *zoom\_in*, and with *focus\_area*.

Model	MME(R)	CharXiv	HR-4K	V*	HalB	InfoVQA
Qwen2.5-VL-7B	652.5	37.6	68.8	77.5	42.1	80.0
w/ general	656.8	38.1	69.2	77.6	42.3	80.3
+ w/ MATHV360K	683.4	39.4	71.3	81.4	42.8	81.2
++ w/ LLaVA-CoT	688.6	39.7	74.9	88.2	44.1	81.4
+++ w/ ArxivQA	<b>702.1</b>	<b>41.8</b>	<b>76.2</b>	<b>90.4</b>	<b>44.4</b>	<b>82.0</b>

Table 6: Impact of training data on model performance: Only MATHV360K, plus LLaVA-CoT-100K, and with ArxivQA.

we introduce perceptual data from LLaVA-CoT-100K, an intervention that elevates the model’s fine-grained perception capability without a trade-off in reasoning performance, specifically improving by 3.6% on HR-Bench 4K and 6.8% on VStarBench. We further expanded the training dataset by incorporating ArxivQA, which consists of challenging abstract diagrams from Arxiv papers, substantially fortifies the model’s logical reasoning faculties despite its narrow data distribution, improving it by 13.5 points on the MME reasoning task and up to 2.1% on CharXiv. Ultimately, the synergistic integration of multi-source, heterogeneous datasets enhances and amplifies the model’s higher-order iterative reasoning capabilities.

## Further Analysis

**Should We Crop, Draw Bbox, or Reuse the Original Images When Focusing on Key Entities or Regions?** During training, we draw bbox on images based on the coordinates returned by the *focus\_area* operation. This stems from the fact that some coordinates only provide approximate focal regions, analogous to human visual attention mechanisms, which may either incompletely cover target instances or excessively include irrelevant areas. Directly cropping images based on samples with incomplete target coverage would lead to critical visual information loss, thereby compromising the reasoning chain integrity.

To identify the optimal image manipulation method when focusing on key entities or regions, we evaluate three *focus\_area* modes—drawing the bbox, image cropping, and reusing the original image—while preserving the functionalities of *zoom\_in* and *reuse*. As shown in Table 7, experimental results demonstrate that the image cropping delivers optimal performance. Specifically, Simple o3 can accurately cover target entities or regions when executing *focus\_area* operations, without producing incomplete crops that trigger “I can’t see” or “I can’t find” responses. This proves that repeatedly injecting key visual information effectively enhances model reasoning capabilities.

Notably, although the input distribution of cropped im-

Method	MME(R)	CharXiv	HR-4K	V*	HalB	InfoVQA
Crop	702.1	<b>41.8</b>	<b>76.2</b>	90.4	<b>44.4</b>	<b>82.0</b>
Draw	698.2	41.2	75.4	<b>90.6</b>	43.8	<b>82.0</b>
Reuse	<b>704.3</b>	40.7	74.2	89.3	43.8	81.8

Table 7: Performance comparison of *focus\_area* operation variants: image cropping, bbox drawing, and original image reusing, based on provided coordinates.

Res	MME(R)	CharXiv	HR-4K	V*	HalB	InfoVQA
Low	699.2	32.4	56.9	61.3	41.5	62.3
Med	<b>702.1</b>	<b>41.8</b>	69.3	78.0	44.4	82.0
High	<b>702.1</b>	40.1	<b>76.2</b>	<b>90.4</b>	<b>46.7</b>	<b>82.6</b>

Table 8: Performance comparison of maximum input resolution variants: low resolution ( $256 \times 28 \times 28$ ), medium resolution ( $2048 \times 28 \times 28$ ), and high resolution ( $16384 \times 28 \times 28$ ).

ages (which may contain only partial entities) differs from the distribution of training data (mostly complete multi-entity images), this discrepancy does not affect model performance. Benefiting from the strong grounding capability of the base model, Simple o3 further unleashes its reasoning potential while learning this interleaved image-text reasoning format. In contrast, while the method of drawing bbox aligns with the training distribution and preserves complete entity information, those redundant visual tokens actually degrade model performance. Reusing the original image yields the poorest results due to the lack of explicit region indication, which tends to scatter attention across irrelevant entities or regions.

## How Does Input Resolution Affect Model Performance?

We explored the impact of the maximum input image resolution on the performance of Simple o3, dividing it into three variants: low resolution, medium resolution, and high resolution. As shown in Table 8, When the maximum input resolution was set to a low level, the model performed poorest—an expected outcome, since excessively low-resolution images impair the model’s fundamental perceptual capabilities. Despite being trained primarily on low-resolution images, the model generalizes well to higher-resolution inputs during inference. On multimodal reasoning benchmarks, medium resolution proved sufficient for capturing core visual elements, and increasing the input from medium to high resolution did not yield significant performance gains. Notably, in the CharXiv task, medium-resolution input even outperformed high-resolution input by 1.7%. This may due to the explosion of visual tokens at high resolutions, which could disrupt the model’s attention allocation across long sequences and hinder effective focus on critical regions. However, high-resolution inputs demonstrably enhanced performance on perception-oriented benchmarks while further reducing hallucination phenomena and improving parsing accuracy in document-based tasks.

## Conclusion

In this work, we present Simple o3, a novel framework that significantly advances multimodal reasoning capabilities through dynamic tool interactions and interleaved vision-language reasoning. By introducing a scalable, low-cost data synthesis pipeline, we curate the high-quality TWI-Tools-146K dataset, establishing a foundation for training models on complex reasoning tasks. Incorporating image masking during training, Simple o3 demonstrates strong performance on diverse benchmarks. Furthermore, we present the first in-depth analysis of how different tools affect model inference performance, providing key insights for advancing the 'thinking with images' paradigm. We found that by introducing additional visual tokens, reusing and magnifying the original image improves the model's visual reasoning and fine-grained perception, while image cropping based on precise visual grounding allows the model to effectively focus on key entities or regions, further enhancing its capabilities. In the future, we will explore more tools and thinking with images with RL training, and extend the paradigm from vision-language reasoning model to vision-language action model.

## References

Alayrac, J.-B.; Donahue, J.; Luc, P.; Miech, A.; Barr, I.; Hasson, Y.; Lenc, K.; Mensch, A.; Millican, K.; Reynolds, M.; et al. 2022. Flamingo: a visual language model for few-shot learning. *Advances in neural information processing systems*, 35: 23716–23736.

Awadalla, A.; Gao, I.; Gardner, J.; Hessel, J.; Hanafy, Y.; Zhu, W.; Marathe, K.; Bitton, Y.; Gadre, S.; Sagawa, S.; et al. 2023. Openflamingo: An open-source framework for training large autoregressive vision-language models. *arXiv preprint arXiv:2308.01390*.

Bai, J.; Bai, S.; Chu, Y.; Cui, Z.; Dang, K.; Deng, X.; Fan, Y.; Ge, W.; Han, Y.; Huang, F.; et al. 2023. Qwen technical report. *arXiv preprint arXiv:2309.16609*.

Bai, S.; Chen, K.; Liu, X.; Wang, J.; Ge, W.; Song, S.; Dang, K.; Wang, P.; Wang, S.; Tang, J.; et al. 2025a. Qwen2. 5-vl technical report. *arXiv preprint arXiv:2502.13923*.

Bai, T.; Hu, Z.; Sun, F.; Qiu, J.; Jiang, Y.; He, G.; Zeng, B.; He, C.; Yuan, B.; and Zhang, W. 2025b. Multi-Step Visual Reasoning with Visual Tokens Scaling and Verification. *arXiv preprint arXiv:2506.07235*.

Chen, K.; Zhang, Z.; Zeng, W.; Zhang, R.; Zhu, F.; and Zhao, R. 2023. Shikra: Unleashing multimodal llm's referential dialogue magic. *arXiv preprint arXiv:2306.15195*.

Chen, L.; Li, J.; Dong, X.; Zhang, P.; Zang, Y.; Chen, Z.; Duan, H.; Wang, J.; Qiao, Y.; Lin, D.; et al. 2024a. Are we on the right way for evaluating large vision-language models? *Advances in Neural Information Processing Systems*, 37: 27056–27087.

Chen, X.; Fang, H.; Lin, T.-Y.; Vedantam, R.; Gupta, S.; Dollár, P.; and Zitnick, C. L. 2015. Microsoft coco captions: Data collection and evaluation server. *arXiv preprint arXiv:1504.00325*.

Chen, Z.; Wang, W.; Cao, Y.; Liu, Y.; Gao, Z.; Cui, E.; Zhu, J.; Ye, S.; Tian, H.; Liu, Z.; et al. 2024b. Expanding performance boundaries of open-source multimodal models with model, data, and test-time scaling. *arXiv preprint arXiv:2412.05271*.

Chung, J.; Kim, J.; Kim, S.; Lee, J.; Kim, M. S.; and Yu, Y. 2025. Don't Look Only Once: Towards Multimodal Interactive Reasoning with Selective Visual Revisitation. *arXiv preprint arXiv:2505.18842*.

Dai, W.; Li, J.; Li, D.; Tiong, A.; Zhao, J.; Wang, W.; Li, B.; Fung, P. N.; and Hoi, S. 2023. Instructblip: Towards general-purpose vision-language models with instruction tuning. *Advances in neural information processing systems*, 36: 49250–49267.

Fan, X.; Ji, T.; Jiang, C.; Li, S.; Jin, S.; Song, S.; Wang, J.; Hong, B.; Chen, L.; Zheng, G.; et al. 2024. Mousi: Poly-visual-expert vision-language models. *arXiv preprint arXiv:2401.17221*.

Fan, Y.; He, X.; Yang, D.; Zheng, K.; Kuo, C.-C.; Zheng, Y.; Narayananaraju, S. J.; Guan, X.; and Wang, X. E. 2025. GRIT: Teaching MLLMs to Think with Images. *arXiv:2505.15879*.

Fu, C.; Chen, P.; Shen, Y.; Qin, Y.; Zhang, M.; Lin, X.; Yang, J.; Zheng, X.; Li, K.; Sun, X.; Wu, Y.; and Ji, R. 2024. MME: A Comprehensive Evaluation Benchmark for Multimodal Large Language Models. *arXiv:2306.13394*.

Ge, C.; Cheng, S.; Wang, Z.; Yuan, J.; Gao, Y.; Song, J.; Song, S.; Huang, G.; and Zheng, B. 2024. Convllava: Hierarchical backbones as visual encoder for large multimodal models. *arXiv preprint arXiv:2405.15738*.

Guan, T.; Liu, F.; Wu, X.; Xian, R.; Li, Z.; Liu, X.; Wang, X.; Chen, L.; Huang, F.; Yacoob, Y.; et al. 2024. Hallusion-bench: an advanced diagnostic suite for entangled language hallucination and visual illusion in large vision-language models. In *Proceedings of the IEEE/CVF Conference on Computer Vision and Pattern Recognition*, 14375–14385.

Guo, D.; Yang, D.; Zhang, H.; Song, J.; Zhang, R.; Xu, R.; Zhu, Q.; Ma, S.; Wang, P.; Bi, X.; et al. 2025. Deepseek-r1: Incentivizing reasoning capability in llms via reinforcement learning. *arXiv preprint arXiv:2501.12948*.

Huang, W.; Jia, B.; Zhai, Z.; Cao, S.; Ye, Z.; Zhao, F.; Xu, Z.; Hu, Y.; and Lin, S. 2025. Vision-r1: Incentivizing reasoning capability in multimodal large language models. *arXiv preprint arXiv:2503.06749*.

Hurst, A.; Lerer, A.; Goucher, A. P.; Perelman, A.; Ramesh, A.; Clark, A.; Ostrow, A.; Welihinda, A.; Hayes, A.; Radford, A.; et al. 2024. Gpt-4o system card. *arXiv preprint arXiv:2410.21276*.

Jin, B.; Zeng, H.; Yue, Z.; Yoon, J.; Arik, S.; Wang, D.; Zamani, H.; and Han, J. 2025. Search-r1: Training llms to reason and leverage search engines with reinforcement learning. *arXiv preprint arXiv:2503.09516*.

Kojima, T.; Gu, S. S.; Reid, M.; Matsuo, Y.; and Iwasawa, Y. 2022. Large language models are zero-shot reasoners. *Advances in neural information processing systems*, 35: 22199–22213.

Li, B.; Zhang, Y.; Guo, D.; Zhang, R.; Li, F.; Zhang, H.; Zhang, K.; Zhang, P.; Li, Y.; Liu, Z.; et al. 2024a. Llava-onevision: Easy visual task transfer. *arXiv preprint arXiv:2408.03326*.

Li, J.; Li, D.; Savarese, S.; and Hoi, S. 2023a. Blip-2: Bootstrapping language-image pre-training with frozen image encoders and large language models. In *International conference on machine learning*, 19730–19742. PMLR.

Li, L.; Wang, Y.; Xu, R.; Wang, P.; Feng, X.; Kong, L.; and Liu, Q. 2024b. Multimodal arxiv: A dataset for improving scientific comprehension of large vision-language models. *arXiv preprint arXiv:2403.00231*.

Li, X.; Zou, H.; and Liu, P. 2025. Torl: Scaling tool-integrated rl. *arXiv preprint arXiv:2503.23383*.

Li, Y.; Du, Y.; Zhou, K.; Wang, J.; Zhao, W. X.; and Wen, J.-R. 2023b. Evaluating Object Hallucination in Large Vision-Language Models. *arXiv:2305.10355*.

Li, Z.; Yang, B.; Liu, Q.; Ma, Z.; Zhang, S.; Yang, J.; Sun, Y.; Liu, Y.; and Bai, X. 2024c. Monkey: Image resolution and text label are important things for large multi-modal models. In *proceedings of the IEEE/CVF conference on computer vision and pattern recognition*, 26763–26773.

Liu, H.; Li, C.; Li, Y.; and Lee, Y. J. 2024a. Improved baselines with visual instruction tuning. In *Proceedings of the IEEE/CVF conference on computer vision and pattern recognition*, 26296–26306.

Liu, H.; Li, C.; Wu, Q.; and Lee, Y. J. 2023. Visual instruction tuning. *Advances in neural information processing systems*, 36: 34892–34916.

Liu, H.; Li, C.; Wu, Q.; and Lee, Y. J. 2024b. Visual instruction tuning. *Advances in neural information processing systems*, 36.

Liu, Y.; Peng, B.; Zhong, Z.; Yue, Z.; Lu, F.; Yu, B.; and Jia, J. 2025a. Seg-zero: Reasoning-chain guided segmentation via cognitive reinforcement. *arXiv preprint arXiv:2503.06520*.

Liu, Y.; Qu, T.; Zhong, Z.; Peng, B.; Liu, S.; Yu, B.; and Jia, J. 2025b. VisionReasoner: Unified Visual Perception and Reasoning via Reinforcement Learning. *arXiv preprint arXiv:2505.12081*.

Liu, Z.; Sun, Z.; Zang, Y.; Dong, X.; Cao, Y.; Duan, H.; Lin, D.; and Wang, J. 2025c. Visual-rft: Visual reinforcement fine-tuning. *arXiv preprint arXiv:2503.01785*.

Lu, S.; Li, Y.; Chen, Q.-G.; Xu, Z.; Luo, W.; Zhang, K.; and Ye, H.-J. 2024. Ovis: Structural embedding alignment for multimodal large language model. *arXiv preprint arXiv:2405.20797*.

Mathew, M.; Bagal, V.; Tito, R.; Karatzas, D.; Valveny, E.; and Jawahar, C. 2022. Infographiccvqa. In *Proceedings of the IEEE/CVF Winter Conference on Applications of Computer Vision*, 1697–1706.

Mathew, M.; Karatzas, D.; and Jawahar, C. 2021. Docvqa: A dataset for vqa on document images. In *Proceedings of the IEEE/CVF winter conference on applications of computer vision*, 2200–2209.

Ni, M.; Yang, Z.; Li, L.; Lin, C.-C.; Lin, K.; Zuo, W.; and Wang, L. 2025. Point-rft: Improving multimodal reasoning with visually grounded reinforcement finetuning. *arXiv preprint arXiv:2505.19702*.

Saikh, T.; Ghosal, T.; Mittal, A.; Ekbal, A.; and Bhattacharyya, P. 2022. Scienceqa: A novel resource for question answering on scholarly articles. *International Journal on Digital Libraries*, 23(3): 289–301.

Shao, H.; Qian, S.; Xiao, H.; Song, G.; Zong, Z.; Wang, L.; Liu, Y.; and Li, H. 2024. Visual cot: Unleashing chain-of-thought reasoning in multi-modal language models. *CoRR*.

Shi, W.; Hu, Z.; Bin, Y.; Liu, J.; Yang, Y.; Ng, S.-K.; Bing, L.; and Lee, R. K.-W. 2024. Math-llava: Bootstrapping mathematical reasoning for multimodal large language models. *arXiv preprint arXiv:2406.17294*.

Su, A.; Wang, H.; Ren, W.; Lin, F.; and Chen, W. 2025. Pixel reasoner: Incentivizing pixel-space reasoning with curiosity-driven reinforcement learning. *arXiv preprint arXiv:2505.15966*.

Team, K.; Du, A.; Gao, B.; Xing, B.; Jiang, C.; Chen, C.; Li, C.; Xiao, C.; Du, C.; Liao, C.; et al. 2025. Kimi k1.5: Scaling reinforcement learning with llms. *arXiv preprint arXiv:2501.12599*.

Wang, Q.; Ding, R.; Zeng, Y.; Chen, Z.; Chen, L.; Wang, S.; Xie, P.; Huang, F.; and Zhao, F. 2025a. VRAG-RL: Empower Vision-Perception-Based RAG for Visually Rich Information Understanding via Iterative Reasoning with Reinforcement Learning. *arXiv preprint arXiv:2505.22019*.

Wang, W.; Ding, L.; Zeng, M.; Zhou, X.; Shen, L.; Luo, Y.; Yu, W.; and Tao, D. 2025b. Divide, conquer and combine: A training-free framework for high-resolution image perception in multimodal large language models. In *Proceedings of the AAAI Conference on Artificial Intelligence*, volume 39, 7907–7915.

Wang, Z.; Xia, M.; He, L.; Chen, H.; Liu, Y.; Zhu, R.; Liang, K.; Wu, X.; Liu, H.; Malladi, S.; et al. 2024. Charxiv: Charting gaps in realistic chart understanding in multimodal llms. *Advances in Neural Information Processing Systems*, 37: 113569–113697.

Wei, J.; Wang, X.; Schuurmans, D.; Bosma, M.; Xia, F.; Chi, E.; Le, Q. V.; Zhou, D.; et al. 2022. Chain-of-thought prompting elicits reasoning in large language models. *Advances in neural information processing systems*, 35: 24824–24837.

Wu, P.; and Xie, S. 2024. V?: Guided visual search as a core mechanism in multimodal llms. In *Proceedings of the IEEE/CVF Conference on Computer Vision and Pattern Recognition*, 13084–13094.

Xu, G.; Jin, P.; Li, H.; Song, Y.; Sun, L.; and Yuan, L. 2024. Llava-cot: Let vision language models reason step-by-step. *arXiv preprint arXiv:2411.10440*.

Xu, W.; Wang, J.; Wang, W.; Chen, Z.; Zhou, W.; Yang, A.; Lu, L.; Li, H.; Wang, X.; Zhu, X.; et al. 2025. Visulogic: A benchmark for evaluating visual reasoning in multi-modal large language models. *arXiv preprint arXiv:2504.15279*.

Ye, J.; Hu, A.; Xu, H.; Ye, Q.; Yan, M.; Xu, G.; Li, C.; Tian, J.; Qian, Q.; Zhang, J.; et al. 2023a. Ureader: Universal ocr-free visually-situated language understanding with multimodal large language model. *arXiv preprint arXiv:2310.05126*.

Ye, Q.; Xu, H.; Xu, G.; Ye, J.; Yan, M.; Zhou, Y.; Wang, J.; Hu, A.; Shi, P.; Shi, Y.; et al. 2023b. mplug-owl: Modularization empowers large language models with multimodality. *arXiv preprint arXiv:2304.14178*.

Yu, Q.; Zhang, Z.; Zhu, R.; Yuan, Y.; Zuo, X.; Yue, Y.; Dai, W.; Fan, T.; Liu, G.; Liu, L.; et al. 2025. Dapo: An open-source llm reinforcement learning system at scale. *arXiv preprint arXiv:2503.14476*.

Yu, W.; Yang, Z.; Li, L.; Wang, J.; Lin, K.; Liu, Z.; Wang, X.; and Wang, L. 2024. MM-Vet: Evaluating Large Multimodal Models for Integrated Capabilities. *arXiv:2308.02490*.

Yuan, Y.; Li, W.; Liu, J.; Tang, D.; Luo, X.; Qin, C.; Zhang, L.; and Zhu, J. 2024. Osprey: Pixel understanding with visual instruction tuning. In *Proceedings of the IEEE/CVF Conference on Computer Vision and Pattern Recognition*, 28202–28211.

Zeng, Y.; Zhang, H.; Zheng, J.; Xia, J.; Wei, G.; Wei, Y.; Zhang, Y.; Kong, T.; and Song, R. 2024. What matters in training a gpt4-style language model with multimodal inputs? In *Proceedings of the 2024 Conference of the North American Chapter of the Association for Computational Linguistics: Human Language Technologies (Volume 1: Long Papers)*, 7930–7957.

Zhang, G.; Zhong, T.; Xia, Y.; Yu, Z.; Li, H.; He, W.; Shu, F.; Liu, M.; She, D.; Wang, Y.; et al. 2025a. Cmmcot: Enhancing complex multi-image comprehension via multi-modal chain-of-thought and memory augmentation. *arXiv preprint arXiv:2503.05255*.

Zhang, J.; Huang, J.; Yao, H.; Liu, S.; Zhang, X.; Lu, S.; and Tao, D. 2025b. R1-vl: Learning to reason with multimodal large language models via step-wise group relative policy optimization. *arXiv preprint arXiv:2503.12937*.

Zhang, X.; Gao, Z.; Zhang, B.; Li, P.; Zhang, X.; Liu, Y.; Yuan, T.; Wu, Y.; Jia, Y.; Zhu, S.-C.; et al. 2025c. Chain-of-Focus: Adaptive Visual Search and Zooming for Multimodal Reasoning via RL. *arXiv preprint arXiv:2505.15436*.

Zheng, Z.; Yang, M.; Hong, J.; Zhao, C.; Xu, G.; Yang, L.; Shen, C.; and Yu, X. 2025. DeepEyes: Incentivizing “Thinking with Images” via Reinforcement Learning. *arXiv preprint arXiv:2505.14362*.

Zhou, H.; Li, X.; Wang, R.; Cheng, M.; Zhou, T.; and Hsieh, C.-J. 2025. R1-Zero’s “Aha Moment” in Visual Reasoning on a 2B Non-SFT Model. *arXiv preprint arXiv:2503.05132*.

Zhu, D.; Chen, J.; Shen, X.; Li, X.; and Elhoseiny, M. 2023. Minigpt-4: Enhancing vision-language understanding with advanced large language models. *arXiv preprint arXiv:2304.10592*.

Zhu, M.; Zhong, H.; Zhao, C.; Du, Z.; Huang, Z.; Liu, M.; Chen, H.; Zou, C.; Chen, J.; Yang, M.; et al. 2025. Active-O3: Empowering Multimodal Large Language Models with Active Perception via GRPO. *arXiv preprint arXiv:2505.21457*.

## Prompt Template for Data Generation

You need to perform image-text interleaved multi-step reasoning according to the "observation-reasoning-operation" paradigm.

1. Observe the current image, then perform atomic logical reasoning for the current round and determine the next visual operation (whether to focus on the key region, zoom in further, or reuse the original image) within `<reasoning>` and `</reasoning>` tags, and return the visual operation parameters.
2. Then, you receive the processed image after the visual operation.
3. Repeat Step 1-2 until sufficient information is obtained.
4. Make a concluding inference within `<reasoning>` and `</reasoning>` tags.
5. Provide the concise and accurate final answer or value within `<answer>` and `</answer>` tags.

- Given the ground truth, you must hide the prior knowledge of the rationale when outputting the complete reasoning path that leads to the ground truth.

- DO NOT MENTION ANY PARAMETERS within the `<reasoning>` and `</reasoning>` tags.
- Ensure the returned function name is semantically aligned with the determined visual operation.
- If you focus on the key region, you should ensure full coverage of all entities targeted for visual operations.
- All image operations are based on the original image.
- Ensure that each round of logical reasoning and visual operation contributes to reaching the ground truth.

The absolute image size is  $(\{w\}, \{h\})$ .

Question: {query}

Answer: {gt}

Figure 3: Prompt template for the reasoning path generator.

```

tools = [
{
  "type": "function",
  "function": {
    "name": "focus_area",
    "description": "returns the bbox of the focused area in the original image using normalized coordinates [ymin, xmin, ymax, xmax] in range of [0, 1000]",
    "parameters": {
      "type": "object",
      "properties": {
        "coordinates": {
          "type": "array",
          "description": "[ymin, xmin, ymax, xmax]",
          "items": {
            "type": "number",
            "minimum": 0,
            "maximum": 1000,
          },
          "minItems": 4,
          "maxItems": 4,
        },
      },
      "required": ["coordinates"],
    },
  },
},
{
  "type": "function",
  "function": {
    "name": "zoom_in",
    "description": "Magnifies image area using interpolation while maintaining original data",
    "parameters": {
      "type": "object",
      "properties": {
        "scale": {
          "type": "number",
          "minimum": 1,
        },
      },
      "required": ["scale"],
    },
  },
},
{
  "type": "function",
  "function": {
    "name": "reuse",
    "description": "Reuses the image without any modifications to enhance visual memory",
  },
},
]

```

Figure 4: Tool definitions in OpenAI's dialogue format.

### Tool Verification Prompt Template (focus\_area)

You are an expert evaluator who is responsible for checking whether the drawn red bounding box matches or encompasses the region of focus in the mentioned visual operation.

- Returns "TRUE" if the red bounding box matches or encompasses the target area/entity.
- Returns "FALSE" if the red bounding box deviates too much from the target area/entity, or is not semantically aligned with the visual operation planning.

NOW EVALUATE THE FOLLOWING:

{res\_text}

The normalized coordinate (range [0, 1000]) of drawn bbox: [{ymin}, {xmin}, {ymax}, {xmax}]

ANSWER WITH "TRUE" OR "FALSE", DO NOT INCLUDE OTHER WORDS!

Figure 5: Tool verification prompt when executing *focus\_area*. The model determines whether the input image and the returned coordinates are semantically aligned with the visual operation planning.

### Tool Verification Prompt Template (reuse & zoom\_in)

You are an expert evaluator who is responsible for checking whether the output JSON argument is semantically consistent with the visual operation planning in the reasoning content? The reasoning process is composed of two components: the atomic reasoning step followed by visual operation planning.

- Returns "TRUE" if the output JSON argument is semantically consistent with the visual operation planning
- Returns "FALSE" if the output JSON argument is not semantically consistent with the visual operation planning

NOW EVALUATE THE FOLLOWING:

Reasoning Content: {res\_text}

JSON Arguments: {arguments}

ANSWER WITH "TRUE" OR "FALSE", DO NOT INCLUDE OTHER WORDS!

Figure 6: Tool verification prompt when executing *reuse* and *zoom\_in*. The model determines whether the returned function is semantically aligned with the visual operation planning.

## Answer Verification Prompt Template

You are an expert evaluator tasked with determining if a SYSTEM'S ANSWER matches the GROUND TRUTH. Please carefully analyze the ground truth and the system's answer based on the question.

Apply the following evaluation criteria, and respond TRUE if:

- Focus on semantic equivalence rather than exact wording
- Allow for paraphrases and different phrasings that convey the same meaning
- Ignore minor grammatical differences or punctuation variations
- For categorical answers, match must be precise unless synonyms are clearly equivalent
- For list-type answers, order doesn't matter unless specified

Input:

Question: [Input Question]

GROUND TRUTH: [The correct reference answer]

SYSTEM ANSWER: [The answer to evaluate]

Output - respond with exactly one word - either "TRUE" or "FALSE":

["TRUE"/"FALSE"]

Now evaluate the following:

Question: {question}

GROUND TRUTH: {gt}

SYSTEM ANSWER: {ans}

ANSWER WITH "TRUE" OR "FALSE", DO NOT INCLUDE OTHER WORDS!

Figure 7: Answer verification prompt. The model judges whether the the system output is accurate based on the question and ground truth.

## System Prompt for Simple o3

You are proficient in interaction with the user.

# Tools

You may call one or more functions to assist with the user query.

You are provided with function signatures within <tools></tools> XML tags:

```
<tools>
  {"type": "function", "function": {"type": "function", "function": {"name": "focus_area", "description": "returns the bbox of the focused area in the original image using absolute coordinates [xmin, ymin, xmax, ymax]", "parameters": {"type": "object", "properties": {"coordinates": {"type": "array", "description": "[xmin, ymin, xmax, ymax]", "items": {"type": "number", "minimum": 0, "minItems": 4, "maxItems": 4}}, "required": ["coordinates"]}}}}
  {"type": "function", "function": {"type": "function", "function": {"name": "zoom_in", "description": "Magnifies image area using interpolation while maintaining original data", "parameters": {"type": "object", "properties": {"scale": {"type": "number", "minimum": 1}}, "required": ["scale"]}}}}
  {"type": "function", "function": {"type": "function", "function": {"name": "reuse", "description": "Reuses the image without any modifications to enhance visual memory"}}}
</tools>
```

For each function call, return a json object with function name and arguments within <function></function> XML tags:

```
<function>
  {"name": <function-name>, "arguments": <args-json-object>}
</function>
```

Figure 8: System prompt for Simple o3. Simple o3 calls the corresponding tool during the inference stage according to the definition, thereby operating the image to complete interleaved visual-language reasoning.

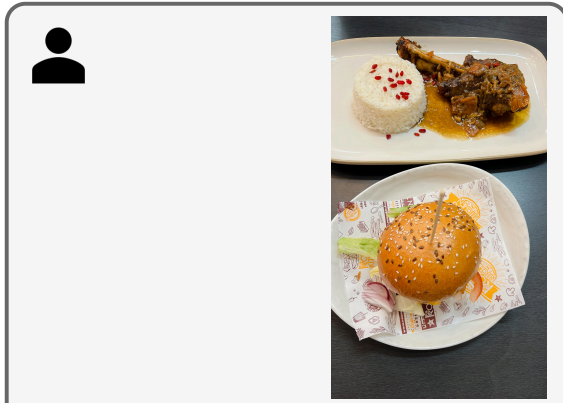
### Tool Command Samples for Simple o3

```
#focus_area
{"name": "focus_area", "arguments": {"coordinates": [0, 386, 419, 643]}}
```

```
#zoom_in
{"name": "zoom_in", "arguments": {"scale": 2}}
```

```
#reuse
{"name": "reuse", "arguments": {}}
```

Figure 9: Examples of three tool commands in JSON format, including *focus\_area*, *zoom\_in*, and *reuse*.



What food is on the table?

<reasoning>

The question asks about the food on the table. The image shows two plates of food. To accurately identify all items, I will first focus on the top plate which contains what appears to be a main dish and rice.

</reasoning>

<function>

{"name": "focus\_area", "arguments": {"coordinates": [0, 0, 923, 768]}}

</function>

<observation>



</observation>

<reasoning>

I have already identified the main dish as a lamb shank and rice from the previous observation. Now I need to identify the food on the bottom plate. I will focus on the bottom plate to get a clearer view of its contents.

</reasoning>

<function>

{"name": "focus\_area", "arguments": {"coordinates": [0, 768, 923, 1679]}}

</function>

<observation>



</observation>

<reasoning>

I have successfully identified both dishes. The top plate has a lamb shank and rice. The bottom plate has a burger. I can now provide the complete answer.

</reasoning>

<answer>

There is a lamb shank and rice on the table, along with a burger.

</answer>



Figure 10: Multi-step interleaved vision-language reasoning of Simple o3 – Case 1. Simple o3 uses atomic reasoning steps to gradually analyze and accurately locate each entity.



<reasoning>

The user is asking whether there is a cow in the image. I will first observe the entire image to get an overall sense of its content. The image appears to be a busy street scene with many buses and buildings. There are no obvious cows visible at first glance. To confirm this, I will reuse the image as it seems clear enough to make a judgment.

</reasoning>

<function>

{"name": "reuse", "arguments": {}}

</function>

<observation>



</observation>

<reasoning>

I have carefully observed the entire image and can confirm that there are no cows present. The image depicts a city street with numerous buses and buildings.

</reasoning>

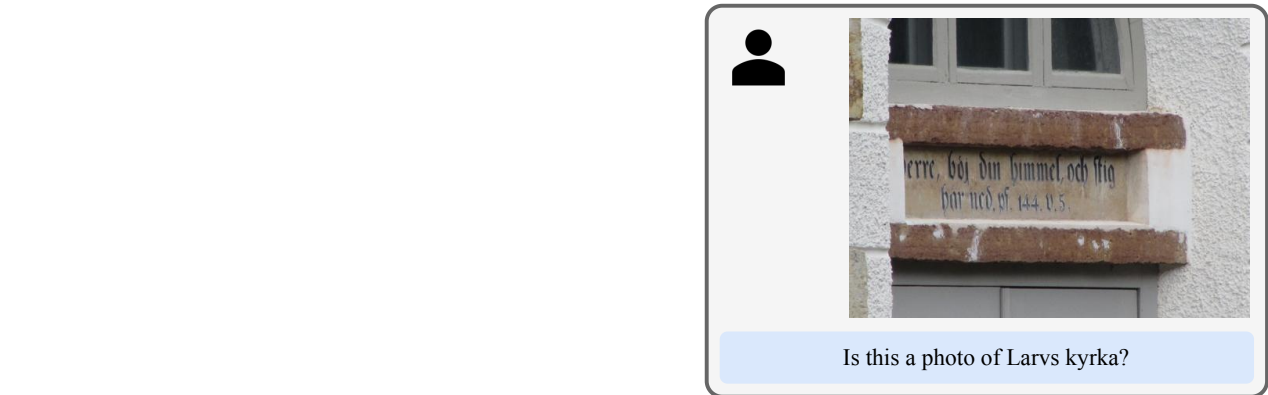
<answer>

No

</answer>



Figure 11: Multi-step interleaved vision-language reasoning of Simple o3 – Case 2. Simple o3 can reconfirm the deduction by reusing the original image.



<reasoning>

The question asks whether the image shows Larvs kyrka. I need to examine the text on the stone plaque to see if it belongs to Larvs Kyrka. The current image shows the entire plaque, but the text is small and difficult to read clearly. Therefore, I will zoom in on the text to make it legible.

</reasoning>

<function>

{"name": "zoom\_in", "arguments": {"scale": 2}}

</function>

<observation>



</observation>

<reasoning>

I have already zoomed in once, but the text is still not clear enough to read. I need to zoom in further to be able to read the text on the stone plaque.

</reasoning>

<function>

{"name": "zoom\_in", "arguments": {"scale": 4}}

</function>

<observation>



</observation>

<reasoning>

I have successfully zoomed in twice. Now the text on the stone plaque is much clearer, which is indeed the stone plaque on Larvs kyrka. This is a quote from the Bible, Psalm 144, verse 5. In English (KJV). This directly answers the question.

</reasoning>

<answer>

yes

</answer>



Figure 12: Multi-step interleaved vision-language reasoning of Simple o3 – Case 3. If Simple o3 detects that certain entities or fonts in an image are too small, it can enhance perception of the current image through iterative magnification.



Is this a photo of St Thomas Rest Park?

<reasoning>

The question asks whether the image shows St Thomas Rest Park. The image displays a large building with a distinctive architectural style, surrounded by greenery. To determine if it's St Thomas Rest Park, I need to identify specific features that might indicate its identity. Since there are no clear signs or distinguishing features visible in the initial view, I will first focus on the entire building to get a better overall sense of its characteristics.

</reasoning>

<function>

{"name": "focus\_area", "arguments": {"coordinates": [0, 0, 531, 391]}}

</function>

<observation>



</observation>

<reasoning>

The image shows a large, old-looking building with multiple stories and dormer windows. It appears to be made of stone and brick, with some parts covered in ivy. There's a paved path leading up to the entrance. Given the question about "St Thomas Rest Park," which sounds like a park or recreational area, and not a typical historical building, I need to look for any clues that might link this building to such a place. However, based on the current view, there are no obvious signs or contextual elements that would definitively identify it as St Thomas Rest Park. Therefore, I will reuse the image as there is no specific area to focus on or zoom into that would provide more information to answer the question.

</reasoning>

<function>

{"name": "reuse", "arguments": {}}

</function>

<observation>



</observation>

<reasoning>

The image depicts an old, multi-story building with a distinctive architectural style, possibly a chateau or manor house, situated in a natural setting with grass and trees. There are no discernible features or signs within the image that explicitly identify it as "St Thomas Rest Park." The architecture does not align with common representations of a rest park, which typically feature open spaces, recreational areas, and modern infrastructure rather than grand historical buildings. Without additional context or information beyond what is visually present, it is impossible to confirm if this is St Thomas Rest Park.

</reasoning>

<answer>

No

</answer>



Figure 13: Multi-step interleaved vision-language reasoning of Simple o3 – Case 4. Simple o3 extends both text tokens and visual tokens simultaneously, further enhancing its reasoning capabilities.